EARTHQUAKE ENGINEERING AND STRUCTURAL DYNAMICS
Earthquake Engng Struct. Dyn. 2000; **29**: 159–176

Dynamic analysis of structures with Maxwell model

Tomohiko Hatada*,†, Takuji Kobori‡, Masatoshi Ishida§ and Naoki Niwa¶

Kobori Research Complex, Kajima Corporation, KI Building, 6-5-30, Akasaka, Minato-ku, Tokyo 107-8502, Japan

SUMMARY

A numerical method has been developed for the dynamic analysis of a tall building structure with viscous dampers. Viscous dampers are installed between the top of an inverted V-shaped brace and the upper beam on each storey to reduce vibrations during strong disturbances like earthquakes. Analytically, it is modelled as a multi-degree-of freedom (MDOF) system with the Maxwell models. First, the computational method is formulated in the time domain by introducing a finite element of the Maxwell model into the equation of motion in the discrete-time system, which is based on the direct numerical integration. Next, analyses for numerical stability and accuracy of the proposed method are discussed. The results show its numerical stability. Finally, the proposed method is applied to the numerical analysis of a realistic building structure to demonstrate its practical validity.

KEY WORDS: Maxwell model; viscous damper; dynamic analysis; direct integration; tall building; stability and accuracy

1. INTRODUCTION

A variety of viscous dampers forming parts of a structural system as supplementary energy dissipation devices have been developed to reduce building responses to dynamic loads such as earthquakes. These systems are composed of simple mechanisms, and effectively reduce building responses [1–8]. The authors have developed a high-performance oil damper providing high-level damping to large structures such as tall buildings, and being highly stable within normal conditions [1–4]. It is installed between the top of an inverted V-shaped brace and the upper beam on each storey to efficiently dissipate earthquake-induced energy. In the structural design considering the system's damping effects, it is indispensable to simulate its behaviour during earthquakes in the time domain through numerical analyses using a mathematical model of the building structure with dampers.

* Correspondence to: Tomohiko Hatada, Senior Research Engineer, Kobori Research Complex, Kajima Corporation, KI Building, 6-5-30, Akasaka, Minato-ku, Tokyo 107-8502, Japan.
† E-mail: hatada@krc.kajima.co.jp
‡ Professor Emeritus of Kyoto University, Chief Executive Adviser of Kajima Corporation
§ Senior Coordinator, Intelligent Systems Department
¶ Senior Research Engineer

CCC 0098–8847/2000/020159–18$17.50

Received 19 March 1999
Accepted 30 July 1999

When the damping coefficient of the damper is larger, we have to consider the equivalent horizontal stiffness of the braces in its analytical model. Consequently, the damper and brace are simply represented as a Maxwell model, in which a dashpot and a stiffness spring are connected in series. When the Maxwell model is directly introduced into the equation of motion of the structural model, it becomes a third-order ordinary differential equation (ODE), which is difficult to solve numerically in terms of numerical stability and accuracy.

Various studies have been reported in the fields of dynamic analyses of structural systems including the Maxwell model in the time domain. They can be roughly divided into two types as:

(1) Solve the third-order ODE directly.
(2) Formulate the system's equation of motion except for the Maxwell model part, and incorporate it into the common second-order ODE as a supplementary force by solving the equation of motion of the Maxwell model.

Among the examples based on the first approach for the analysis of structures modelled as MDOF systems, Chen *et al.* [11], have reported a method using a modal superposition analysis in the frequency domain through Laplace transformation. This method can be used to solve the equation of motion of the system including the Maxwell models; however, it is difficult to deal with system non-linearity in the time domain. Malone *et al.* [12] have reported a method setting a new degree-of-freedom at mass-less point between a dashpot and a stiffness spring of the Maxwell model, and then apply a common numerical integration scheme. In this method, it is necessary to consider twice the degrees-of-freedom of the original system. The reports on the second approach have been mainly applied to the analyses of material stress–strain relationships. Kitagawa *et al.* [13] have reported the analysis of reinforced concrete elements by considering the effect of strain speed. They treated the Maxwell model as a supplementary restoring force on the equation of motion of the system discretized by a central difference method, which is categorized into an explicit integration scheme. Similarly, on the response analysis of a reinforced concrete frame structure including the Maxwell model, Fujimoto *et al.* [14] have reported a computational method in which a restoring force of the Maxwell model is substituted by an equivalent tangent stiffness and a correction force through the convergence calculation process, and those equivalent variables are introduced into the equation of motion discretized by Newmark's β method. Among the examples in this approach, on the analysis of the stress–strain relationship of a visco-elastic body, restoring force of the Maxwell model is incorporated into the incremental form of the equation of motion based on the finite element method [15–19]. Considering the dynamic analyses of MDOF systems such as a tall building from the practical viewpoint of structural design, it is desirable to analyse it in the time domain by incorporating the Maxwell models directly into the common second-order ODE of the simple analytical model. Among the past reports, Hatada *et al.* [9] have presented a computational method formulated for that purpose; however, its numerical stability and accuracy were not theoretically clarified.

This paper presents a numerical method in the time domain for an MDOF system including the Maxwell models. The proposed method is developed to simulate the behaviour of tall buildings equipped with viscous dampers. First, the computational method is formulated by introducing a finite element of the Maxwell model into the second-order ODE in the discrete-time system, which is based on the direct numerical integration. Next, theoretical analyses for the numerical stability and accuracy of the proposed method are discussed. The results show that this method is numerically stable. Finally, the examples of the numerical analysis of a realistic building structure demonstrate the practical validity of the proposed numerical method.

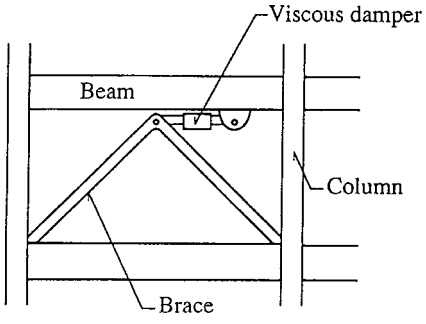

Figure 1. Example of installation of the viscous damper [1, 2].

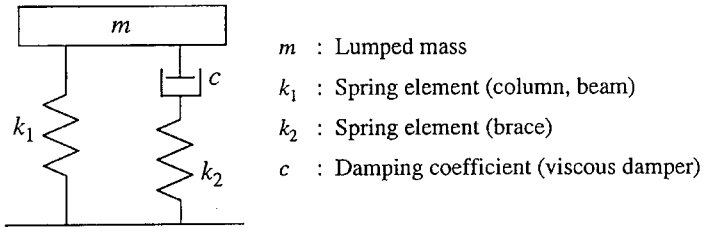

Figure 2. There-element Maxwell model.

2. FORMULATION OF COMPUTATIONAL METHOD

2.1. Three-element Maxwell model

The objective model structure is shown in Figure 1. Viscous dampers are installed between the top of an inverted V-shaped brace and the upper beam on each storey [1–4, 9]. In the dynamic analysis of this object during earthquakes, the damper and brace are simply represented by a Maxwell model, in which a dashpot and a stiffness spring are connected in series. In formulating the computational method for its dynamic analysis, let us assume a three-element Maxwell model as the basic analytical model, where the Maxwell model is arranged parallel to a spring element representing column and beam stiffness.

Figure 2 shows a schematic diagram of the three-element Maxwell model, where the building structure is simplified as a lumped mass m with stiffness k_1, k_2, and damping c. The equilibrium equations for this structure excited by an external force $f(t)$ are as follows:

$$m\ddot{x}(t) + p(t) + k_1 x(t) = f(t) \tag{1}$$

$$\dot{p}(t) + \frac{k_2}{c} p(t) = k_2 \dot{x}(t) \tag{2}$$

where $x(t)$ and $p(t)$ are the displacement of the mass and the restoring force of the Maxwell model, respectively. By eliminating $\dot{p}(t)$ and $p(t)$ using Equations (1) and (2) after differentiating both sides

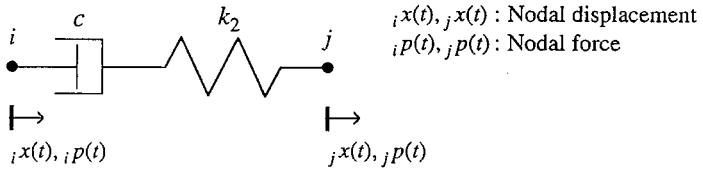

Figure 3. Maxwell model.

of Equation (1), the equation of motion of the system can be expressed in the following form:

$$m\dddot{x}(t) + \frac{mk_2}{c}\ddot{x}(t) + (k_1 + k_2)\dot{x}(t) + \frac{k_1 k_2}{c}x(t) = \dot{f}(t) + \frac{k_2}{c}f(t) \tag{3}$$

Considering the computational methods for Equation (3), the direct approach is to reduce the order of the equation to second-order through transformation of variables [10]. Another approach is to rewrite Equation (3) into a 2DOF's second-order ODE after setting a new degree-of-freedom at mass-less point between a dashpot and a stiffness spring of the Maxwell model, and then apply a common numerical integration scheme [12]. However for both methods, it is necessary to rewrite the original form of the analysis method based on the common second-order ODE of motion, and to consider twice the degrees-of-freedom of the original system.

2.2. Finite element of Maxwell model

The computational method is formulated by incorporating a finite element of the Maxwell model into the second-order ODE of motion in the discrete-time system. Figure 3 shows the Maxwell model, where $_i x(t)$ and $_j x(t)$ denote its nodal displacements, and $_i p(t)$ and $_j p(t)$ denote the nodal forces, respectively. When $x(t) = {}_j x(t) - {}_i x(t)$ and $p(t) = {}_i p(t) = {}_j p(t)$, the equation of motion is given by Equation (2). To solve Equation (2) in the discrete time system, the following two cases are considered: the case in which $\dot{x}(t)$ on the right-hand side is assumed to be a consistent variation during each time interval, and the case in which $\dot{p}(t)$ on the left-hand side is similarly assumed.

Case-1: $\dot{x}(t)$ is assumed to be a consistent variation in a time interval. When Equation (2) is solved for $p(t)$, the general solution is as follows:

$$p(t) = \exp\left(-\frac{k_2 t}{c}\right)\left\{k_2 \int_0^t \left[\dot{x}(t)\exp\left(\frac{k_2 t}{c}\right)\right] dt + p(0)\right\} \tag{4}$$

where $p(0)$ is the initial value of $p(t)$. Now, let us consider Equation (4) in the discrete time system. First, let x_n and p_n denote $x(t)$ and $p(t)$ at time t_n, and Δt be the time increment between t_n and t_{n+1}. If it is assumed that $\dot{x}(t)$ varies linearly during each time increment Δt as shown in Figure 4(a), the velocity during this interval is given as

$$_n\dot{x}(t) = \dot{x}_n + \frac{\dot{x}_{n+1} - \dot{x}_n}{\Delta t}t, \quad t \in (0, \Delta t) \tag{5}$$

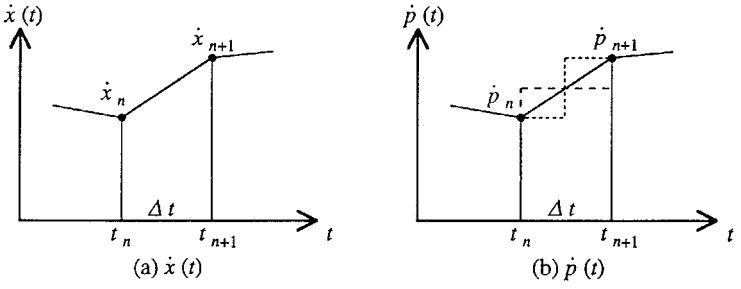

Figure 4. Consistent variations of Maxwell model response in a time interval: (a) $\dot{x}(t)$; (b) $\dot{p}(t)$.

where ${}_n\dot{x}(t)$ is the velocity between t_n and t_{n+1}. Equation (4) can be rewritten between t_n and t_{n+1} in the discrete time system as follows:

$$p_{n+1} = \exp\left(-\frac{k_2\,\Delta t}{c}\right)\left\{k_2\int_0^{\Delta t}\left[{}_n\dot{x}(t)\exp\left(\frac{k_2\,t}{c}\right)\right]\mathrm{d}t + p_n\right\} \tag{6}$$

By integrating the right-hand side of Equation (6) after substituting Equation (5), and rearranging that expression, the final solution of Equation (2) in the discrete time system can be expressed as

$$p_{n+1} = {}_{\mathrm{A}}\alpha\dot{x}_{n+1} + {}_{\mathrm{A}}\beta\dot{x}_n + {}_{\mathrm{A}}\gamma p_n \tag{7a}$$

where

$${}_{\mathrm{A}}\alpha = c\left[1 + \frac{c}{k_2\Delta t}\left\{\exp\left(-\frac{k_2\Delta t}{c}\right) - 1\right\}\right] \tag{7b}$$

$${}_{\mathrm{A}}\beta = -c\left[\exp\left(-\frac{k_2\Delta t}{c}\right) + \frac{c}{k_2\Delta t}\left\{\exp\left(-\frac{k_2\Delta t}{c}\right) - 1\right\}\right] \tag{7c}$$

$${}_{\mathrm{A}}\gamma = \exp\left(-\frac{k_2\Delta t}{c}\right) \tag{7d}$$

Let us call it Method-A here, to distinguish from the following case.

Case-2: *$\dot{p}(t)$ is assumed to be a consistent variation in a time interval.* If it is assumed that $\dot{p}(t)$ varies linearly during each time increment Δt as shown in Figure 4(b), p_{n+1} is expressed in terms of p_n, $\dot{p}_{n+1}$, and $\dot{p}_n$ as

$$p_{n+1} = p_n + \frac{\Delta t}{2}(\dot{p}_{n+1} + \dot{p}_n) \tag{8}$$

As shown in Figure 4(b), during each time increment, when $\dot{p}(t)$ is assumed to be a linear variation, a step function at each nth step, or a step function in the middle of each time increment, p_{n+1} can be similarly expressed as Equation (8). After eliminating $\dot{p}_{n+1}$ from the direct discretized from of Equation (2) by using Equation (8), the final solution of Equation (2) in the discrete time system can be expressed as

$$p_{n+1} = {}_{\mathrm{B}}\,\alpha\dot{x}_{n+1} + {}_{\mathrm{B}}\beta\dot{x}_n + {}_{\mathrm{B}}\gamma p_n \tag{9a}$$

where

$$_{\mathrm{B}}\alpha = \frac{ck_2\,\Delta t}{2c + k_2\Delta t} \tag{9b}$$

$$_{\mathrm{B}}\beta = \frac{ck_2\,\Delta t}{2c + k_2\Delta t} \tag{9c}$$

$$_{\mathrm{B}}\gamma = \frac{2c - k_2\,\Delta t}{2c + k_2\Delta t} \tag{9d}$$

Let us call this case Method-B.

The difference between Methods A and B comes from the assumption in each time interval, but both methods define a restoring force of the Maxwell model in the discrete time system. Expressing Equation (7a) and (9a) in terms of the nodal forces, i.e. velocities and displacements of Maxwell model, yields the following form as

$$\begin{Bmatrix} {}_ip \\ {}_jp \end{Bmatrix}_{n+1} = \begin{bmatrix} \alpha & -\alpha \\ -\alpha & \alpha \end{bmatrix} \begin{Bmatrix} {}_i\dot{x} \\ {}_j\dot{x} \end{Bmatrix}_{n+1} + \begin{bmatrix} \beta & -\beta \\ -\beta & \beta \end{bmatrix} \begin{Bmatrix} {}_i\dot{x} \\ {}_j\dot{x} \end{Bmatrix}_n + \begin{bmatrix} \gamma & 0 \\ 0 & \gamma \end{bmatrix} \begin{Bmatrix} {}_ip \\ {}_jp \end{Bmatrix}_n \tag{10a}$$

where

$$\text{Method-A:} \quad \alpha = {}_{\mathrm{A}}\alpha, \quad \beta = {}_{\mathrm{A}}\beta, \quad \gamma = {}_{\mathrm{A}}\gamma \tag{10b}$$

$$\text{Method-B:} \quad \alpha = {}_{\mathrm{B}}\alpha, \quad \beta = {}_{\mathrm{B}}\beta, \quad \gamma = {}_{\mathrm{B}}\gamma \tag{10c}$$

In the equation of motion of the system in the discrete time system, the Maxwell model is treated as a finite element expressed as Equation (10a). It is realized by substituting the first-term matrix composed of α's on the right-hand side into a damping matrix and considering the other terms as a correction force, which can be computed by response values at one step prior to the current step. For the proposed method, total degrees-of-freedom do not increase to more than those of the original analytical model even when considering the Maxwell model.

2.3. Procedure of the numerical scheme

Let us formulate the procedure of the numerical scheme for the three-element Maxwell model shown in Figure 2 in the discrete time system. By substituting Equation (7a) or (9a) for a finite element of the Maxwell model into a discretized from of Equation (1), the equation of motion is expressed as

$$m\ddot{x}_{n+1} + \alpha\dot{x}_{n+1} + k_1 x_{n+1} = f_{n+1} - \beta\dot{x}_n - \gamma p_n \tag{11}$$

where α, β and γ are the terms expressed in Equation (10b) or (10c). p_n on the right-hand side is a restoring force of the Maxwell model at the nth step, obtained from Equation (7a) or (9a). Equation (11) is a second-order ODE, and it can be solved through the step-by-step process by a common numerical integration scheme. When an implicit method, e.g. Newmark's β method, is applied to the direct numerical integration scheme, the step-by-step process consists of the following operations:

(1) Compute the response values of the mass, $\ddot{x}_{n+1}$, $\dot{x}_{n+1}$ and x_{n+1} at time t_{n+1} by Newmark's formula using the known values, $\ddot{x}_n$, $\dot{x}_n$, x_n and p_n at time t_n and the external force f_{n+1} at time t_{n+1}.

(2) Compute the restoring force of Maxwell model p_{n+1} at time t_{n+1}, from Equation (7a) or (9a) using $\dot{x}_{n+1}$, $\dot{x}_n$ and p_n.
(3) Process (1) is then repeated for the next time interval.

The procedure is formulated for the basic three-element Maxwell model, but it can be easily developed to a more complicated MDOF system. Furthermore, it can be applicable to non-linear structural systems by regarding its motion as sequences of successively changing linear systems, on the assumption that damping and stiffness properties remain constant during each time interval and those tangent slopes at each time instant are used in each computation process.

3. NUMERICAL STABILITY AND ACCURACY

3.1. Analysis process

The numerical stability and accuracy of the proposed method are discussed quantitatively in this section using the three-element Maxwell model shown in Figure 2. In this analysis, Newmark's β method with $\beta = \frac{1}{4}$, commonly applied to the dynamic analysis of buildings during earthquakes, is chosen for the direct numerical integration scheme to solve the equation of motion in the discrete time system. The velocity and displacement of the mass at the $(n+1)$th step are given as

$$\dot{x}_{n+1} = \dot{x}_n + \frac{\Delta t}{2}(\ddot{x}_{n+1} + \ddot{x}_n) \tag{12}$$

$$x_{n+1} = x_n + \Delta t \dot{x}_n + \frac{\Delta t^2}{4}(\ddot{x}_{n+1} + \ddot{x}_n) \tag{13}$$

Numerical stability and accuracy are evaluated considering the free vibration of the system expressed as Equation (11), where the external force f_{n+1} is equal to 0. First, let us express the equation of motion in the following recursive form using Equation (7a) or (9a), (11)–(13) as

$$\mathbf{z}_{n+1} = \mathbf{A}\mathbf{z}_n \tag{14a}$$

where

$$\mathbf{z}_n = \{\ddot{x}_n, \dot{x}_n, x_n, p_n\}^{\mathrm{T}} \tag{14b}$$

$$\mathbf{A} = \begin{pmatrix} A_1 & A_2 & A_3 & A_4 \\ \frac{\Delta t}{2}(A_1+1) & \frac{\Delta t}{2}(A_2+1) & \frac{\Delta t}{2}A_3 & \frac{\Delta t}{2}A_4 \\ \frac{\Delta t^2}{4}(A_1+1) & \frac{\Delta t^2}{4}A_2 + \Delta t & \frac{\Delta t^2}{4}A_3 + 1 & \frac{\Delta t^2}{4}A_4 \\ \frac{\Delta t}{2}\alpha(A_1+1) & \alpha\left(\frac{\Delta t}{2}A_2 + 1\right) + \beta & \frac{\Delta t}{2}\alpha A_3 & \frac{\Delta t}{2}\alpha A_4 + \gamma \end{pmatrix} \tag{14c}$$

$$A_1 = -\frac{1}{D}\left(\frac{\Delta r}{2}\alpha + \frac{\Delta t^2 k_1}{4}\right), \quad A_2 = -\frac{1}{D}(\alpha + \beta + \Delta t k_1), \quad A_3 = -\frac{k_1}{D}, \quad A_4 = -\frac{\gamma}{D} \tag{14d}$$

$$D = m + \frac{\Delta t}{2}\alpha + \frac{\Delta t^2 k_1}{4} \tag{14e}$$

and **A** is called an amplification matrix. The numerical stability and accuracy are determined by the eigenvalues $\boldsymbol{\lambda} = \{\lambda_1, \lambda_2, \lambda_3, \lambda_4\}^{\mathrm{T}}$ of the amplification matrix **A**. [26–28]. They are plotted on the complex z-plane in the discrete time system, and their properties can be visualized through the transformation into the complex s-plane in the continuous time system.

3.1.1. Transformation of the eigenvalues. Let one of the eigenvalue vectors $\boldsymbol{\lambda}$ be λ_i, and its transformed eigenvalue in the continuous time system be d_i. Let us write them as

$$\lambda_i = \xi_i + j\eta_i \tag{15a}$$

$$d_i = a_i + jb_i \tag{15b}$$

where j is an imaginary operator. The relationship between λ_i and d_i can be expressed in the following form from the relationship between $\mathbf{z}_{n+1}$ and $\mathbf{z}_n$ in the discrete time system, and the corresponding relationship between $\mathbf{z}(t + \Delta t)$ and $\mathbf{z}(t)$ in the continuous time system [27].

$$\lambda_i = \exp(\Delta t d_i) \tag{16}$$

λ_i can be expressed in the different form by rewriting Equation (15a) as

$$\lambda_i = \rho_i \exp(j\Phi_i) \tag{17a}$$

where

$$\rho_i = \sqrt{\xi_i^2 + \eta_i^2} \tag{17b}$$

$$\Phi_i = \arctan\left(\frac{\eta_i}{\xi_i}\right) \tag{17c}$$

Substituting Equation (15b) into Equation (16) and comparing the real and imaginary parts of λ_i between Equations (16) and (17a), the relationship for each part between λ_i and d_i can be expressed as

$$a_i = \frac{\ln(\rho_i)}{\Delta t} \tag{18a}$$

$$b_i = \frac{\Phi_i}{\Delta t} \tag{18b}$$

3.1.2. Numerical stability. The stability can be discussed in terms of the spectral radius $\rho = \max\{|\lambda_1|, |\lambda_2|, |\lambda_3|, |\lambda_4|\}$ in the discrete time system. When $\rho \leqslant 1$, the system is unconditionally stable, being equivalent to $a_i \leqslant 1$ for all i's in the continuous time system.

3.1.3. Accuracy. Among the eigenvalue vector $\boldsymbol{\lambda}$ of **A**, there is a pair of complexs conjugate roots $\lambda_{1,2} = {}_p\xi \pm j_p\eta$, called principal roots, defining the vibration components of the system. The accuracy can be analysed using the numerical circular frequency $\bar{\omega}$ and the damping factor $\bar{h}$ of the system derived from $\lambda_{1,2}$.

Let $d_{1,2}$ be the corresponding eigenvalues for $\lambda_{1,2}$ in the continuous time system. Its real part ${}_pa$ and the imaginary part ${}_pb$ have the following relationship in terms of $\bar{\omega}$ and $\bar{h}$ as

$${}_pa = -\bar{h}\bar{\omega} \tag{19a}$$

$${}_pb = \bar{\omega}\sqrt{1 - \bar{h}^2} \tag{19b}$$

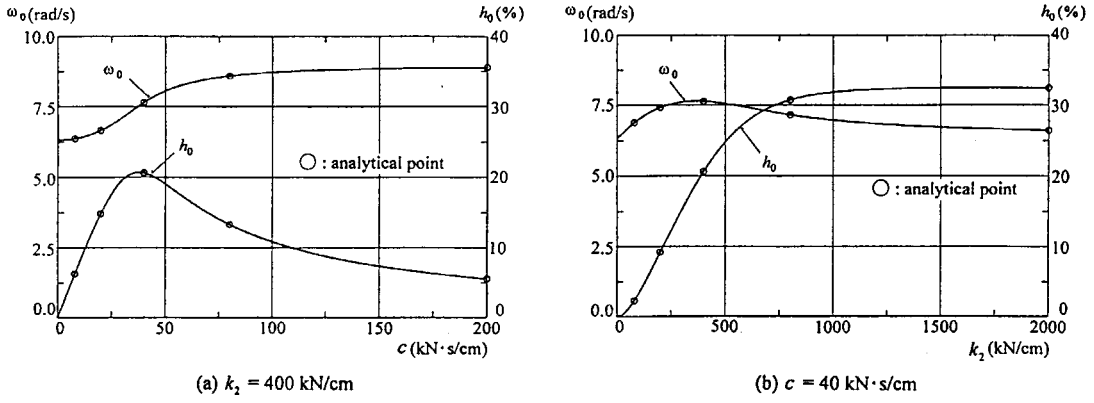

Figure 5. Circular frequencies and damping factors for the three-element Maxwell model: (a) $k_2 = 400$ kN/cm; (b) $c = 40$ kN s/cm.

From Equations (18a), (18b), (19a) and 19(b), the numerical circular frequency $\bar{\omega}$ and damping factor $\bar{h}$ of the system can be expressed as

$$\bar{\omega} = \frac{\sqrt{\ln^2({}_p\rho) + {}_p\Phi^2}}{\Delta t} \tag{20a}$$

$$\bar{h} = \frac{-\ln({}_p\rho)}{\sqrt{\ln^2({}_p\rho) + {}_p\Phi^2}} \tag{20b}$$

where ${}_p\rho$ and ${}_p\Phi$ for the principal roots, i.e. ${}_p\xi$ and ${}_p\eta$, are given by Equations (17b) and (17c). The accuracy can be quantitatively analysed by comparing $\bar{\omega}$ and $\bar{h}$ with the exact natural circular frequency ω_0 and damping factor h_0, respectively.

3.2. *Selection of analysis parameters*

The characteristics of the three-element Maxwell model are defined by the ratio of the stiffness k_1 and k_2 and the damping coefficient c. To qualitatively examine its characteristics, the basic analytical model as shown in Figure 2 is adopted, where the mass m is 980t and the stiffness k_1 is 400 kN/cm. Its characteristics are examined for the parameters k_2 and c.

The natural circular frequency ω_0 and the damping factor h_0 of this model are shown in Figure 5. When c increases under the fixed k_2, h_0 tends to increase to their peaks and then decrease. ω_0 also increases as c increases, which corresponds to the change of the system from stiffness k_1 to stiffness $(k_1 + k_2)$. In the region where the curvature of h_0 is large, that of ω_0 is also large. Next, when k_2 increases under the fixed c, h_0 increases to their peaks and then stays constant. ω_0 also increases to their peaks and then gradually decreases.

Based on these results, the analytical model parameters are chosen at $c = 8$, 20, 40, 80, 200 kN s/cm with $k_2 = 400$ kN/cm, and $k_2 = 80$, 200, 400, 800, 2000 kN/cm with c = 40 kN s/cm indicated as symbol 'o' in Figure 5. The numerical stability and accuracy are analysed for the time increment Δt.

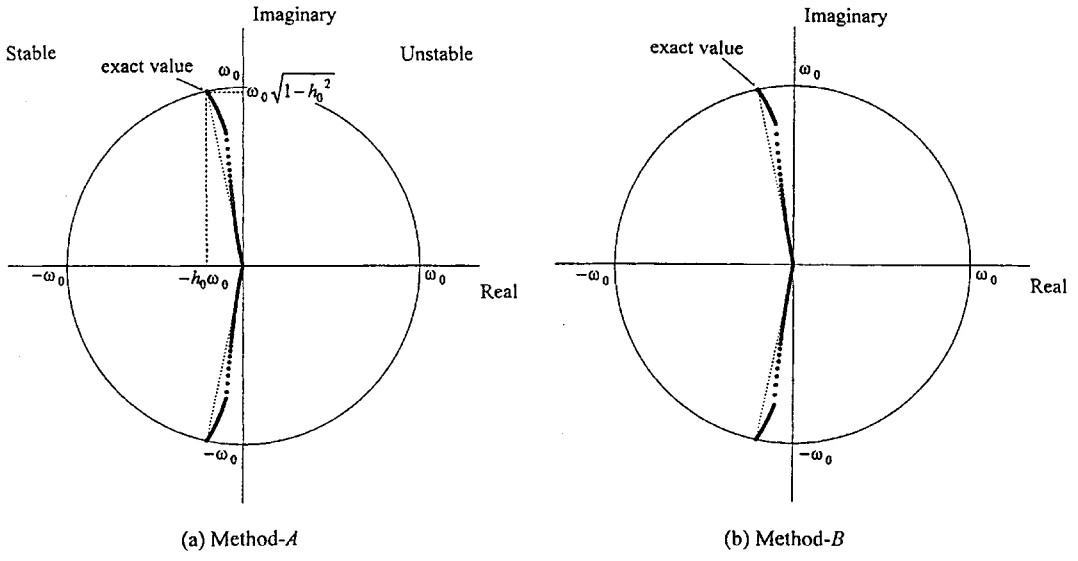

Figure 6. Locus of the eigenvalues of the amplification matrix in the s-plane ($k_2 = 400$ kN/cm, $c = 40$ kN s/cm, $\omega_0\Delta t = 0$–100): (a) Method-A; (b) Method-B.

3.3. Results of the analysis

In Figure 6, the root locus of a pair of complex conjugate eigenvalues of **A** are plotted on the s-plane for the case $k_2 = 400$ kN/cm and $c = 40$ kN s/cm. Each locus has eigenvalues corresponding to the normalized circular frequency $\omega_0\Delta t$ up to 100 with an increment 0.1. $\omega_0\Delta t$ is defined by the multiplication of the exact circular frequency ω_0 and the time increment Δt. The locus shapes for Methods A and B are similar, and both loci lie in the left half of the s-plane, indicating that both methods are stable for these parameters. With the increase of Δt, both the numerical circular frequency $\bar{\omega}$ and damping factor $\bar{h}$ tend to decrease compared to the exact values ω_0 and h_0.

In Figures 7 and 8, the spectral radius ρ, the ratio of circular frequencies $\bar{\omega}/\omega_0$ and the ratio of damping factors $\bar{h}/h_0$ are plotted against $\omega_0\Delta t$. Figure 7 shows the results where c is the analysis parameter for $k_2 = 400$ kN/cm, and Figure 8 shows the results where k_2 is the analysis parameter for $c = 40$ kN s/cm. ρ is less than 1 up to $\omega_0\Delta t = 100$ for each case, indicating that both Method-A and B are numerically stable. $\bar{\omega}/\omega_0$ and $\bar{h}/h_0$ tend to decrease as Δt increases, and the numerical errors by Method-A vary relatively widely for different analytical models compared to the results of Method B. This trend is remarkable for $\bar{h}/h_0$. However, in the region where $\omega_0\Delta t$ is sufficiently small, the numerical errors are negligible and there is little difference between the two methods.

For the application of this method, let us consider the equivalence of these results to the analysis of building structures. For example, the numerical errors in $\bar{\omega}$ and $\bar{h}$ are less than 1 per cent when $\omega_0\Delta t$ is less than about 0.25, and less than 0.2 per cent when $\omega_0\Delta t$ is less than about 0.1. The case of $\omega_0\Delta t = 0.1$ corresponds to the analytical case where, for example, the period of the building is one second and $\Delta t = 0.016$ or where the period of the building is three seconds and $\Delta t = 0.048$.

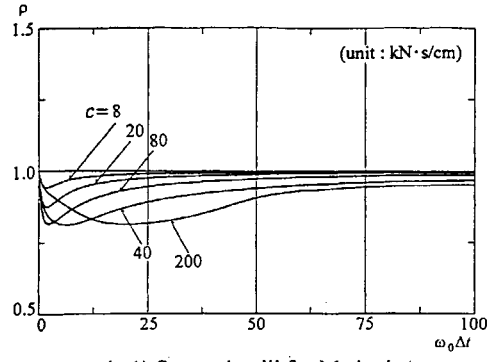

(a-1) Spectral radii for Method-*A*

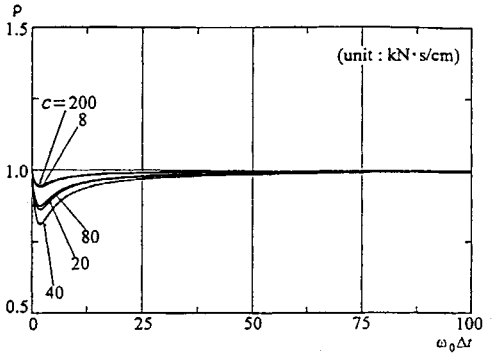

(b-1) Spectral radii for Method-*B*

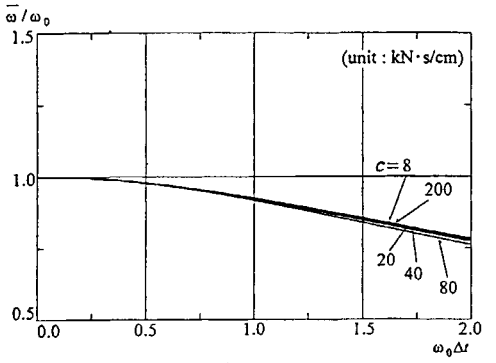

(a-2) Ratios of natural circular frequency for Method-*A*

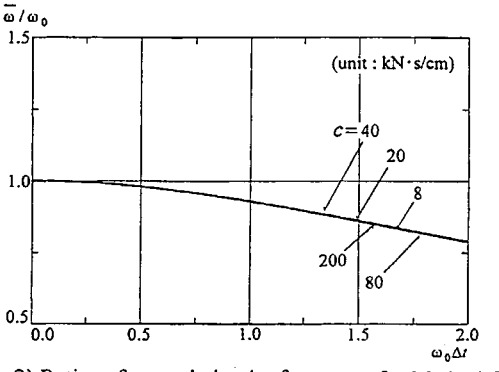

(b-2) Ratios of natural circular frequency for Method-*B*

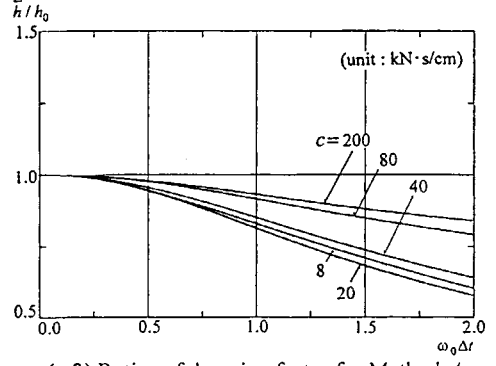

(a-3) Ratios of damping factor for Method-*A*

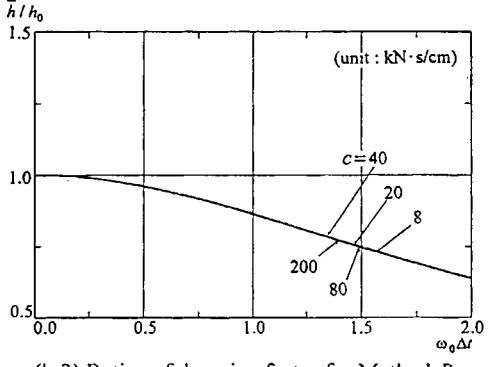

(b-3) Ratios of damping factor for Method-*B*

Figure 7. Analysis of stability and accuracy for varying c ($k_2 = 400$ kN/cm): (a-1) Spectral radii for Method-A; (a-2) Ratios of natural circular frequency for Method-A; (a-3) Ratios of damping factor for Method-A; (b-1) Spectral radii for Method-B; (b-2) Ratios of natural circular frequency for Method-B; (b-3) Ratios of damping factor for Method-B.

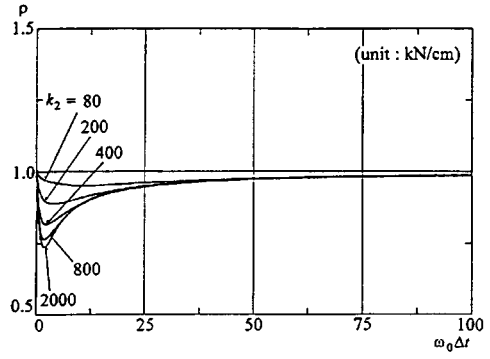

(a-1) Spectral radii for Method-*A*

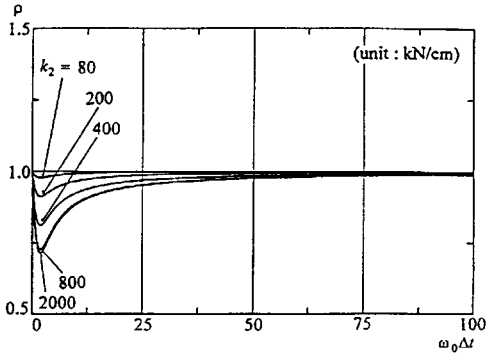

(b-1) Spectral radii for Method-*B*

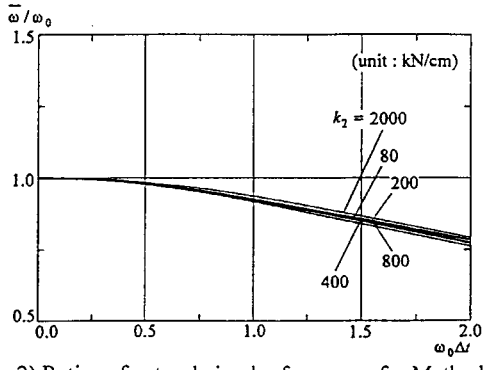

(a-2) Ratios of natural circular frequency for Method-*A*

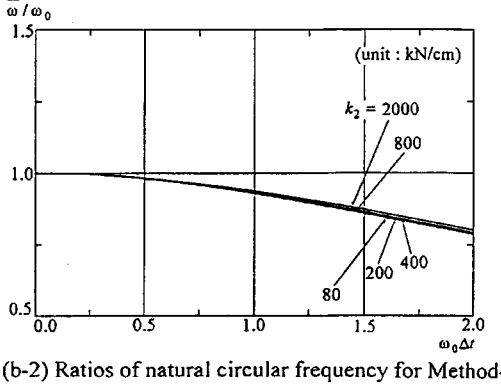

(b-2) Ratios of natural circular frequency for Method-*B*

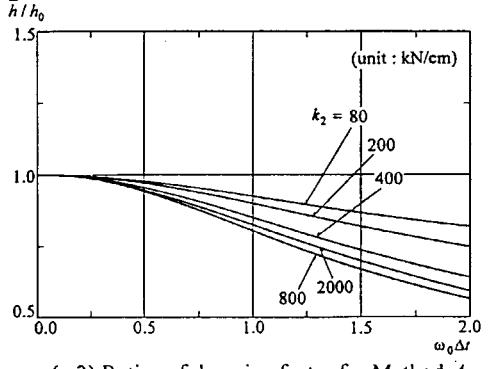

(a-3) Ratios of damping factor for Method-*A*

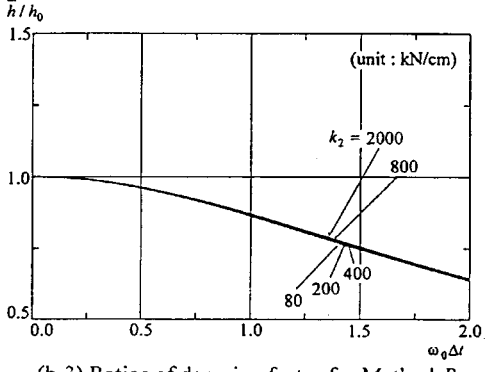

(b-3) Ratios of damping factor for Method-*B*

Figure 8. Analysis of stability and accuracy for varying k_2 ($c = 40$ kN s/cm): (a-1) Spectral radii for Method-A; (a-2) Ratios of natural circular frequency for Method-A; (a-3) Ratios of damping factor for Method-A; (b-1) Spectral radii for Method-B; (b-2) Ratios of natural circular frequency for Method-B; (b-3) Ratios of damping factor for Method-B.

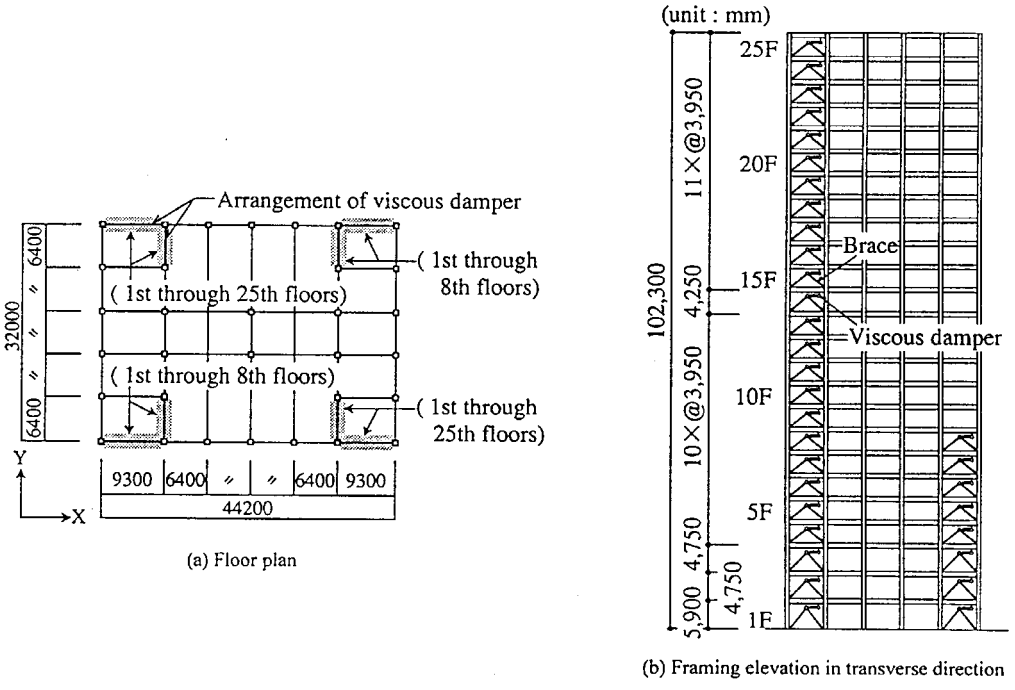

Figure 9. Outline of the building: (a) Floor plan; (b) Framing elevation in the transverse direction.

The discussion developed here is applicable to that of MDOF systems by considering its behaviour through the modal superposition analysis. Furthermore, it is applicable to the analysis of non-linear structural systems by regarding its motion as sequences of successively changing linear systems, on the assumption that damping and stiffness properties remain constant during each time interval and those tangent slopes at each time instant are used in each computation process.

4. NUMERICAL SIMULATION

4.1. Objective model building structure

The validity of the proposed method is discussed through numerical simulations for a realistic building structure [1,2]. The floor plan and framing elevation of the objective model building are shown in Figure 9. It is a 25-storey steel-frame structure with viscous dampers installed between the top of an inverted V-shaped brace and the upper beam on each story as shown in Figure 1. It is 102 m high, and the total mass is 22871 ton. The damping coefficient of each viscous damper is 490 k N s/cm, and their number is 132.

For the analysis, the objective building is modelled as a multi-lumped mass vibration system. Under the rigid floor assumption, the freedom is represented on each floor level, and each weight is represented by a concentrated mass for lateral inertia force. The structural frame, consisting of

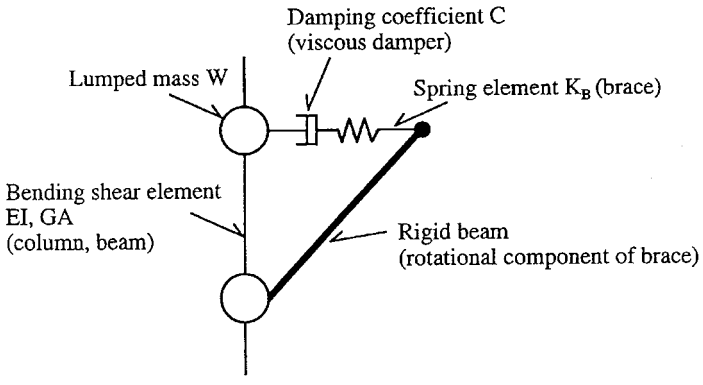

Figure 10. Analytical model.

columns and beams, is represented by bending shear elements. The braces are represented by equivalent spring elements connected to a rigid beam expressing the rotational component of the brace. The viscous dampers are represented by dashpots, and they are inserted between the mass and the spring element. As a result, the analytical model includes the Maxwell model between each adjacent pair of masses. The analytical model is shown in Figure 10, and the details of model parameters are shown in Table I.

The investigation is performed for the transverse Y-direction. The internal viscous damping is assumed to be 2 per cent for the first natural period of the building, representing the inherent damping of the building structure. The primary natural periods and damping factors determined by the complex eigenvalue analysis are given below. Obtained damping factors are about 10–20 per cent for each mode.

Mode	Natural period (s)	Damping factor (%)
1	3.17	12.5
2	0.95	20.3
3	0.53	21.4

Dynamic analyses are performed in the time domain for this analytical model. For the numerical method, Method-B is used for the Maxwell model element, and Newmark's β method with $\beta = \frac{1}{4}$ is adopted for the direct integration method.

4.2. Results of the analysis

First, the accuracy of the proposed method is checked by using a test input motion. The test is conducted by inputting a sinusoidal wave and then inducing a free vibration. The sinusoidal wave is given the following properties: its circular frequency is equal to the first natural frequency ω_1 of the analytical model and the amplitude is unity. This sinusoidal wave is applied for seven cycles as an input ground acceleration, and then the free vibration is induced for three cycles. Figure 11(a) shows the displacement time histories of the top floor for difference Δt's. For comparison, the

Table I. Details of analytical model.

Storey	Mass W (t)	Damping coefficient C (kN s/cm)	Spring constant K_B (kN/cm)	Bending stiffness EI($\times 10^{11}$ kN cm^2)	Shear stiffness GA ($\times 10^3$ kN)
R	1568	980	5410	1194	3405
25	880	980	5410	1749	3183
24	880	980	5410	2058	3151
23	880	980	5410	2223	3263
22	880	980	5410	2284	3199
21	880	980	5410	2326	3390
20	880	980	5410	2655	3659
19	880	980	5410	2655	3699
18	880	980	5410	2655	3699
17	880	980	5410	2655	3707
16	880	980	5410	2634	3723
15	1010	980	5027	3025	3731
14	880	980	5410	3005	3937
13	880	980	5410	2984	4001
12	880	980	5410	2984	4025
11	880	980	5410	2964	4088
10	880	980	5410	3663	4302
9	880	1960	10809	3643	4334
8	880	1960	10809	3602	4366
7	880	1960	10809	3581	4366
6	880	1960	10809	3540	4533
5	880	1960	10809	4198	4795
4	873	1960	9643	4260	5969
3	870	1960	9643	4239	6541
2	950	1960	7800	4528	8192
1					

response computed for $\Delta t = 0.0002$ by setting a new degree-of-freedom at mass-less point between the dashpot and the spring element of the Maxwell model is plotted in the same figure as the exact solution. The response for $\Delta t = 0.02$ ($\omega_1 \Delta t \cong 0.04$) agrees almost exactly with the exact one. For $\Delta t = 0.01$($\omega_1 \Delta t \cong 0.20$), a slight error is recognized. Next, to check the numerical stability of the proposed method, another test is conducted in the same way with larger Δt. In this test, the sinusoidal wave is given the following properties: the circular frequency is equal to $1/5\omega_1$ and the amplitude is unity. The sinusoidal wave is applied for 10 cycles (157 s) and Δt is set to 2 seconds ($\omega_1 \Delta t \cong 4$). Figure 11(b) shows the displacement time history of the top floor. Even for such a large Δt, the response does not show a divergent tendency.

Next, let us investigate the response analysis for the recorded earthquake motion. The El Centro (1940 NS) component is adopted for the input ground motion with the maximum velocity standardized to 25 cm/s. Δt is set to 0.02 s. This value is the one commonly used for the dynamic analysis of buildings of this scale. The response of typical floors for ten seconds are shown in Figure 12, with the exact one defined above. For a random input motion like earthquakes, the responses agree very well with the exact solution, and no errors are recognized on the time histories. In this case, $\omega_1 \Delta t$, $\omega_2 \Delta t$ and $\omega_3 \Delta t$ are between 0.04 and 0.24, and the errors in both

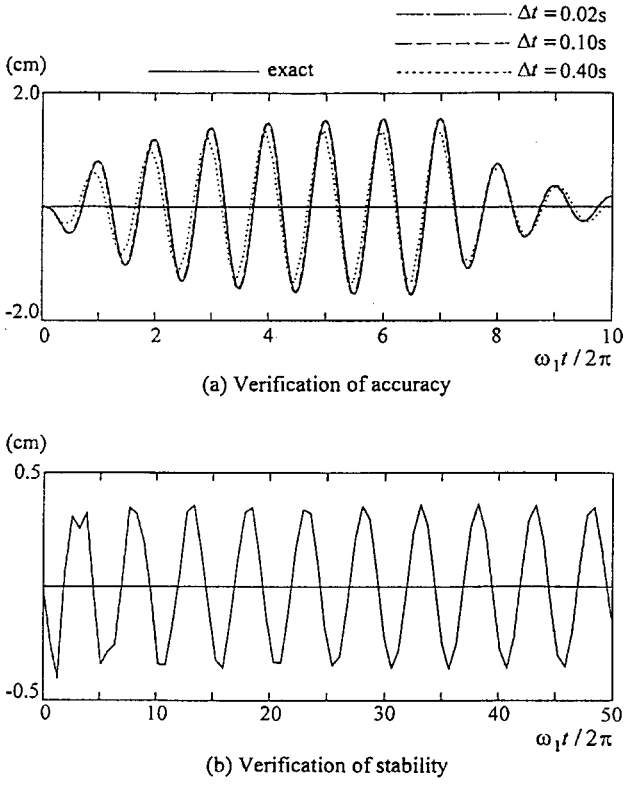

Figure 11. Displacement of the top floor to harmonic ground motion: (a) Verification of accuracy; (b) Verification of stability.

numerical circular frequency $\bar{\omega}$ and damping factor $\bar{h}$ are estimated at between 0.01 and 1.0 per cent for the first–third modes from the results of Section 3. The analysis results show that the responses are not affected by these small errors.

5. CONCLUSIONS

This paper presented a numerical method for the dynamic analysis of tall building structures with viscous dampers in the time domain. Analytically, it is modelled as the MDOF system with the Maxwell models. The computational method is formulated by introducing a finite element of the Maxwell model into the second-order ODE of motion in the discrete-time system, which is based on the direct numerical integration. For the proposed method, total degrees-of-freedom are the same as those of the original analytical model. Next, sufficient numerical stability and accuracy were analytically confirmed for the proposed numerical method. Finally, the numerical simulations for a realistic building structure demonstrate the practical validity of the proposed method. Consequently, the proposed method is useful for the dynamic analyses of structures with the

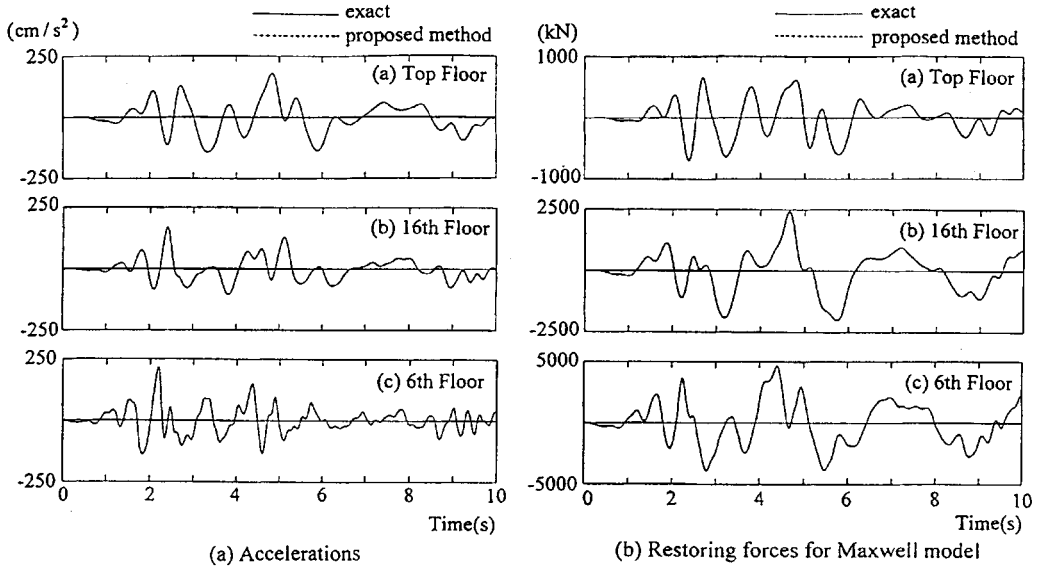

Figure 12. Response of the typical floors to El Centro: (a) Accelerations; (b) Restoring forces for Maxwell model.

Maxwell models; e.g. tall building structures where high-performance viscous dampers or visco-elastic dampers are installed as energy dissipation devices.

REFERENCES

1. Kobori T. Application of the high damping device (HiDAM) to high-rise buildings. *Journal of Structural Engineering Institute., IABSE* 1992; **2**:178–179.
2. Niwa N et al. Passive seismic response controlled structure with high damping device. *Earthquake Engineering Structural Dynmics* 1995; **5**:655–671.
3. Kurata N et al. An experimental study on framed structure with high damping system - shaking tablet test of a three-story steel model. *Journal of Structural Engineering Japan*, 1992; **38B**:235–243.
4. Matsunaga Y et al. High damping device (HiDAM) for response control of large structures. *Proceedings Pressure Vessels and Piping Conference ASME*: Denver, CO, 1993; 69–76.
5. Hanson RD. Supplemental damping for improved seismic performance. *Earthquake Spectra, EERI* 1993; **9**: 319–334.
6. School R. Fundamental design issues for supplemental damping applications. *Earthquake Spectra, EERI* 1993; **9**: 627–636.
7. Miyazaki M, Mitsusaka Y. Design of a building with 20% or greater damping. *Proceedings* 10*th World Conference Earthquake Engng.*, Madrid, Spain, 1992; 4143–4148.
8. Mahmoodi P et al. Performance of viscoelastic dampers in World trade center towers. *Proceedings* 5*th Structural Congress. ASCE*: Orlando, FL, 1987:632–644.
9. Hatada T et al. Study on dynamic analysis of structures with Maxwell model. *Proceedings* 9*th Japan Earthquake Engineering Symposium*, Tokyo, Japan, 1994; 1843–1848.
10. Foss KA. Coordinates which uncouple the equations of motion of damped linear dynamic systems. *Journal of Applied Mechanics ASME* 1958; **32**: 361–364.
11. Chen Q, Zhu D. Vibration analysis theory and application to elastic–viscoelastic composite structures. *Computational Structures* 1990; **37**: 585–595.
12. Malone DW, Connor JJ. Transient dynamic response of linearly viscoelastic structures and continua. *Proceedings Structural Dynamics Aeroelasticity Specialist Conference. AIAA*: New Orleans, LA, 1969; 349–356.

13. Kitagawa Y, Nagataki Y, Kashima T. Dynamic response analysis with effects of strain rate and stress relaxation. *Transaction of Architecture Institute* Japan 1984; **343**:32–41.
14. Fujimoto M, Wada A, Kimura Y. Dynamic response analysis of reinforced concrete frame using a three-element-Maxwell model. *Journal of Structure and Construction Engineering* Japan, 1989; **399**:9–17.
15. Partom Y, Schanin I. Modeling nonlinear viscoelastic response. *Polymer Engineering Science* 1983; **23**:849–859.
16. Amejima S, Fujii T, Nishida H. A simple numerical method for dynamic analysis of adhesive bonded sandwich beams. *Report Science Engineering*, *Doshisha Univ*. Japan, 1987; **27**:21–37.
17. Carol J, Murcia J. A model for the non-linear time-dependent behaviour of concrete on compression based on a Maxwell chain with exponential algorithm. *Materials and Structures* 1989; **22**:176–184.
18. Tuah H. Leonard JW. Dynamic response of viscoelastic cable elements. *Ocean Engineering* 1990; **17**: 23–34.
19. Argyris J, Doltsinis I St. da Silva VD. Constitutive modelling and computation of non-linear viscoelastic solids. part-I: Rheological models and numerical integration techniques. *Computational Methods in Applied Mechanical Engineering* 1991; **88**: 135–163.
20. Yamada Y. Constitutive modelling of inelastic behavior and numerical solution of nonlinear problems by the finite element method. *Computational Structure* 1978; **8**: 533–543.
21. Williams ML. Structural analysis of viscoelastic materials. *J. AIAA* 1964; **2**:785–808.
22. Kolsky H. The role of experimental in the development of solid mechanics – some examples. *Advanced Applied Mechanics*, 1976; **16**:309–368.
23. Sawano T, Kida T, Sudo M. Shear vibration response in a layer of viscoelastic body composed of non-linear spring and Maxwell model. *Report Research Institute Industrial Tech*., *Nihon Univ* 30, Japan, 1989.
24. Fung YC. *Foundations of solid mechanics*, Prentice-hall, Englewood Cliffs, NJ. 1965.
25. Newmark NM. A method of computational for structural dynamics. *Journal of Engineering Mechanics Division ASCE* 1959; **85**:67–94.
26. Belytschko T, Hughes TJR. (eds) *Computational Methods for Transient Analysis*. North-Holland: Amsterdam, 1983.
27. Hilber HM, Hughes TJR, Tailor RL. Improved numerical dissipation for time integration algorithms in structural dynamics. *Earthquake Engineering and Structure Dynamics* 1977; **5**:283–292.
28. Hilbert HM, Hughes TJR, Collocation, dissipation and 'overshoot' for time integration schemes in structural dynamics. *Earthquake Engineering and Structural Dynamics* 1978; **6**:99–117.

